Acta Materialia 178 (2019) 1–9

Contents lists available at ScienceDirect

Acta Materialia

journal homepage: www.elsevier.com/locate/actamat

Full length article

# Segregation-driven grain boundary spinodal decomposition as a pathway for phase nucleation in a high-entropy alloy

Linlin Li [a, b, *], Zhiming Li [a], Alisson Kwiatkowski da Silva [a], Zirong Peng [a], Huan Zhao [a], Baptiste Gault [a, c], Dierk Raabe [a, **]

[a] Max-Planck-Institut für Eisenforschung, Max-Planck-Strasse 1, 40237, Düsseldorf, Germany
[b] Institute of Metal Research, Chinese Academy of Science, Wenhua Road 72, Shenyang, 110016, PR China
[c] Department of Materials, Royal School of Mine, Imperial College London, London, SW7 2AZ, UK

ARTICLE INFO

*Article history:*
Received 29 May 2019
Received in revised form
25 July 2019
Accepted 28 July 2019
Available online 30 July 2019

*Keywords:*
High entropy alloys
Grain boundary segregation
Compositional modulation
Spinodal decomposition
Atom-probe tomography

ABSTRACT

Elemental segregation to grain boundaries (GBs) can induce structural and chemical transitions at GBs along with significant changes in material properties. The presence of multiple principal elements interacting in high-entropy alloys (HEAs) makes the GB segregation and interfacial phase transformation a rather challenging subject to investigate. Here, we explored the temporal evolution of the chemistry for general high-angle GBs in a typical equiatomic FeMnNiCoCr HEA during aging heat treatment through detailed atom probe tomography (APT) analysis. We found that the five principal elements segregate heterogeneously at the GBs. More specifically, Ni and Mn co-segregate to some regions of the GBs along with the depletion of Fe, Co and Cr, while Cr is enriched in other regions of the GBs where Ni and Mn are depleted. The redistribution of these elements on the GBs follow a periodic characteristic, spinodal-like compositional modulation. The accumulation of elements at the GBs can create local compositions by shifting their state from a solid solution (like in the adjacent bulk region) into a spinodal regime to promote interfacial phase-like transitions as segregation proceeds. These results not only shed light on phase precursor states and the associated nucleation mechanism at GBs in alloy systems with multiple principal elements but also help to guide the microstructure design of advanced HEAs in which formation of embrittling phases at interfaces must be avoided.



## 1. Introduction and motivation

High entropy alloys (HEAs) are a class of materials with multiple elements in similar fractions, mostly forming solid solutions with high configurational entropy [1,2]. Their compositions lie in the centers instead of the corners of multi-component phase diagrams and are characterized by high compositional disorder with a wide variety of possible atomic neighborhood configurations. HEAs are of scientific interest because some of them show attractive properties such as excellent toughness at cryogenic temperatures [3], high strain hardening [3,4], good resistance to hydrogen embrittlement [5] and high-temperature stability [6]. Among these, the FeMnNiCoCr HEA is a well-established reference material of single-phase solid solution. This alloy has been studied in detail particularly with respect to its microstructure, mechanical properties and thermodynamic stability [1,3,7–9].

A grain boundary (GB) is an interface between two grains of identical crystal structure but different orientations. They are the most ubiquitous type of planar imperfections in polycrystalline materials [10]. They influence many mechanical and functional properties of materials including strength [11,12], ductility [13], conductivity [14], corrosion [15] and magnetism [16]. Consequently, controlling the structural and chemical states of GBs, which are directly linked to these properties [17], has become an important microstructure design strategy [18]. Segregation engineering has for example been used to enhance GB cohesion [19] or lower interface energy for stabilizing nanocrystals [20] and hence to endow materials with higher strength. Therefore, it is essential to understand the mechanisms that lead to segregation, chemical

* Corresponding author. Max-Planck-Institut für Eisenforschung, Max-Planck-Strasse 1, 40237, Düsseldorf, Germany.
** Corresponding author.
*E-mail addresses:* l.li@mpie.de (L. Li), d.raabe@mpie.de (D. Raabe).

https://doi.org/10.1016/j.actamat.2019.07.052
1359-6454/

ordering, interfacial decomposition and second phase nucleation at GBs [21–24]. This also applies to HEAs with multiple principal elements that can lead to various types of such chemistry-dependent GB phenomena.

Chemical segregation at interfaces is a process driven by the minimization of the system's free energy. It proceeds via partitioning of solute elements to GBs up to the composition at which local equilibrium between bulk and GB is established. Enhanced or reduced interface compositions produced by segregation mark individual and spatially confined thermodynamic states. Interfacial adsorption and concomitant transformations have been experimentally observed and further confirmed by hybrid Monte Carlo (MC) and molecular dynamics (MD) simulations in Si-Au and Ni-Mo alloys [25,26]. The often-observed preference of phase nucleation at GBs is not only associated with the high interface transport coefficients or the low energy barrier for heterogeneous nucleation but also with interface-specific compositional and partitioning precursor states which may substantially deviate from those in the grain interior [27–30]. Similar phenomena have been studied in detail for bulk precipitation phenomena in alloys such as Al-Cu or Al-Mg-Zn-Cu systems [31–33]. In these materials, formation of the stable bulk $Al_2Cu$ or $Mg(Al,Zn,Cu)_2$ phases is preceded by several nano-sized spinodal intermediate precipitation states in the grain interiors [31–33].

GBs are of few interatomic distances in thickness and hence their structure and chemical composition are challenging to investigate. Yet, recent progress in atomic-scale characterization techniques using aberration-corrected scanning transmission electron microscopy (STEM) and atom probe tomography (APT) reveals structural and chemical features of interfaces that were not readily visible previously [21,27,34,35]. For example, STEM observations showed that periodic segregation of Gd exists along twin boundaries in Mg alloys [34]. The segregations of Bi can lead to the formation of ordered superstructures along interfaces in Bi-doped polycrystalline Ni [21]. APT investigations recently also revealed that Gibbsian segregation of Mn to dislocations and GBs in Fe-Mn alloys could induce low-dimensional, confined spinodal fluctuations that act as precursors for austenite nucleation [27]. However, these studies were conducted only in traditional binary or dilute alloy systems but not in the highly concentrated HEAs. The presence of multiple principal elements interacting in HEAs can on the one hand significantly alter the GB segregation and transformation pathway [36], and on the other hand make the atomic scale investigations on the segregations and corresponding interactions of multiple elements at interfaces rather challenging.

Based on the above considerations, in the current study, we investigated the GB segregation, phase nucleation and formation of precursor states from compositional modulations in a fully recrystallized FeMnNiCoCr alloy. APT technique was employed to map the chemistry of a set of general high-angle GBs in this alloy of as-received annealed state and under different aging time. The detailed characteristics of GB segregations, including the elements, their respective degrees of segregation and the in-plane segregation patterns have been determined. Ni and Mn co-segregate while Cr, Fe and Co are depleted at general high-angle GBs; these solute decorations are not homogeneous but form spinodal-like compositional modulations. These segregation and decomposition phenomena can develop into spinodal patterns which act as precursor states to phase nucleation at the GBs. The present results expand our knowledge on GB segregation and interfacial phase transformation mechanisms in alloy systems with multiple principal elements, which provide implications for the design of new HEAs by integration of the role on internal interfaces and other defects such as dislocations.

## 2. Materials and experiments

The FeMnNiCoCr HEA ingot was cast in a vacuum induction furnace from high purity constituent metals of similar fractions. The exact chemical composition of this alloy measured by wet-chemical analysis is $Fe_{18.9}Mn_{19.9}Ni_{20.6}Co_{20.1}Cr_{20.5}$ (at. %). Hot rolling at 900 °C with a thickness reduction ratio of 50% and subsequent annealing at 1200 °C for 24 h were performed to homogenize the material. Afterwards, cold-rolling to a thickness reduction ratio of 60% and annealing at 900 °C for 10 min were performed to refine the grain size. To study the GB segregation behavior of the multiple principal elements in different stages, these samples were aged in Ar atmosphere at 450 °C for 6, 18 and 48 h, respectively. The sample obtained after the annealing at 900 °C is named as the annealed state, while the samples heat-treated at 450 °C for different time are denoted as the aged samples in the following description.

The microstructures of all samples were characterized by using electron backscattering diffraction (EBSD) in a Zeiss 1540 XB scanning electron microscope (SEM). The working distance was 13 mm and the acceleration voltage was 15 kV with an aperture of 120 μm in diameter. The chemical composition was investigated at the sub-nanometer scale by APT using a LEAP™ 3000X HR (Cameca Instruments Inc.). Needle-shaped specimens for APT were fabricated using a dual beam focused-ion-beam (FIB) instrument (FEI Helios Nanolab600/600i) by an in-situ lift-out method. APT measurements were conducted in voltage mode at 70 K, with a pulse fraction of 15%, a pulse rate of 200 kHz, and a target detection rate of 0.4% (4 detection events per 1000 pulses in average). The reconstruction of 3D atom maps, visualization and all data analysis were performed using the IVAS® 3.6.14 software package.

The in-plane composition maps of GBs were also computed in MATLAB (Mathworks Inc.) using an in-house developed analysis approach described in details in Ref. [37]. To put simply, first, this method proceeds by conducting a cluster identification using a K-nearest neighbor method applied to the APT dataset, which allows to extract the Ni or Mn atoms that are segregated along the GB. Second, the highest local point densities amongst these clustered atoms are determined and used to establish the GB plane. In a third step, Voronoi tessellation is applied to divide the entire dataset into sub-volumes. Hereafter, within each subvolume, a one-dimensional composition profile is computed along the normal direction of the GB plane, and the peak value is extracted from this profile and considered to represent the local concentration of Ni or Mn at this location along the GB plane, which is used to plot a two-dimensional GB composition map.

## 3. Results

### 3.1. Microstructure and GB chemistry in the annealed state

Fig. 1(a) shows the starting microstructure and GB characteristics of the FeMnNiCoCr HEA after annealing at 900 °C for 10 min by using EBSD analyses. The grain size for the annealed HEA is about 9 μm and it remains stable over the following course of aging at 450 °C. With the help of SEM and EBSD mapping, needle-shaped specimens for APT measurements containing general high-angle GBs were prepared by using FIB. In general, interstitial atoms such as C and B can diffuse faster than substitutional elements and thus are the first to decorate the GBs [38–40]. In the as-received sample, there are clear enrichments of C and B impurities at a high-angle GB. The C reaches ~0.2 at. % and B reaches ~0.1 at. % in concentration, which are higher than that in the grain interior where the concentration of C is about 0.02 at. % while that of B is less than a few ppm. As a principal substitutional element, Ni also segregates modestly to the GB here, as highlighted by a 26.5 at. % Ni iso-composition surface (Fig. 1(c))

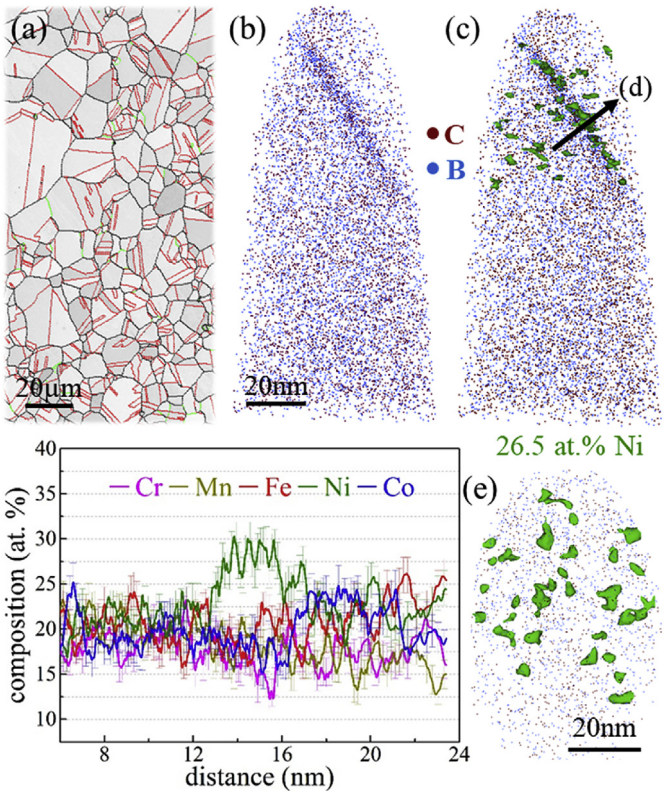


**Fig. 1.** Microstructure and composition of the annealed FeMnNiCoCr alloy. (a) IQ + GB map (low-angle GBs: green, twin boundaries: red, high-angle GBs: black). (b) C and B atomic distribution map obtained from APT. (c) 26.5 at. % Ni iso-composition surface together with C and B atoms. (d) The one-dimensional composition profile along the direction indicated in (c). (e) Normal view of the GB area with 26.5 at. % Ni iso-composition surface. The GB is viewed edge-on in (b) and (c). IQ: Image quality; GB: grain boundary; APT: Atom Probe Tomography. (For interpretation of the references to color in this figure legend, the reader is referred to the Web version of this article.)

and by the one-dimensional composition profile (Fig. 1(d)) (computed across the GB along the arrow in Fig. 1(c)). The same in-plane iso-composition surface viewed from the perspective of the GB normal in Fig. 1(e) (in comparison with the edge-on views in Fig. 1(b and c)) reveals that Ni forms small and isolated Ni-rich islands spreading across the GB plane.

### 3.2. GB segregation and depletion in the aged states

Isothermal aging at 450 °C for up to 48 h leads to pronounced redistribution of the elements at the GBs. Fig. 2 shows the chemical composition of a high-angle GB in a sample aged for 6 h. As C and B impurities always decorate the GBs first, we used them as tracers to mark the GB's position (Fig. 2(a)). An edge-on view of a GB with decorations highlighted by iso-composition surfaces with respective thresholds of 22 at. % Cr and 26 at. % Ni in Fig. 2(b) shows that Cr and Ni segregate to the GB. Fig. 2(c) and (d) display the one-dimensional composition profile across the GB, computed along the light-red and light-blue arrows in Fig. 2(b), respectively. The vertical dashed lines indicate the approximate position of the GB. Fig. 2(c) reveals that Cr segregates to the GB with the peak concentration increasing to ~29 at. %, about 1.5 times of that in the bulk, contrasting with some depletion of Ni and Mn along this section of the same boundary. Fig. 2(d) shows the compositions of the segregation from a nearby location across the GB, revealing an opposite behavior. That is, Ni and Mn segregate to the GBs with their peak concentrations increasing to ~33 at. % and 25 at. %, respectively, about 60% higher relative to their bulk concentrations, while Fe, Co and Cr are substantially depleted. The above observations demonstrate that at the same GB, co-depletion of Fe, Co and Cr and co-segregation of Ni and Mn occur simultaneously within some regions, while segregation of Cr and co-depletion of Ni and Mn occur at the same time in the other regions.

Similar trends of an opposite GB enrichment for Fe, Co and Cr on the one hand and for Ni and Mn on the other hand, can also be observed in samples aged at 450 °C for longer time in Fig. 3 (18 h) and Fig. 4 (48 h). Figs. 3(a) and Fig. 4(a) indicate that C and B atoms also mark the GB position in these two aged states. The 22 at. % Cr and 26 at. % Ni iso-composition surfaces in Figs. 3(b) and Fig. 4(b) highlight the segregations of Cr and Ni to GBs. The one-dimensional composition profiles along the light-red arrow across the GB show that Cr segregates (with the peak concentration of ~26 at. %) with the concurrent depletion of Ni and Mn (Fig. 3(c) and Fig. 4(c)). In the other regions of the same GB, the one-dimensional composition profiles along the light-blue arrow across the GB reveal that Ni and Mn segregations occur accompanied by the co-depletion of Fe, Co and Cr (Figs. 3(d) and Fig. 4(d)). The peak concentrations of Ni and Mn have reached ~53 at. % and ~38 at. %, respectively in the sample aged for 18 h (Fig. 3(d)) which are higher than those at the GB in the sample aged for 6 h. In contrast, Ni and Mn exhibit stronger segregation to the GB with the respective maximum concentrations reaching ~54 at. % and 50 at. % of a large volume in the sample aged for 48 h (Fig. 4(d)), implying the nucleation of NiMn phase.

These analyses all confirm that in the same GB plane co-segregation of Ni and Mn prevails at positions where Fe, Co and Cr are depleted jointly while the opposite behavior (co-depletion of Ni, Mn and segregation of Cr) takes place at other locations. These highly localized enrichments and depletions along the GB plane encouraged us to conduct a more systematic analysis of the in-plane segregation patterns.

### 3.3. In-plane GB segregation patterns in the aged states

Fig. 5 and Fig. 6 display the in-plane composition patterns of high-angle GBs viewed along the normal to the GB plane. The in-plane iso-composition surfaces for 25 at. % Ni (Fig. 5(a)) and 21.5 at. % Mn (Fig. 5(b)) reveal a compositional patterning within the GB plane in the sample aged at 450 °C for 6 h. Aging induces strong co-segregation of Ni and Mn, on the one hand, and Co, Cr and Fe on the other hand, which takes the form of a network made of slightly elongated features. Although the enrichment of Mn does not coincide perfectly with that of Ni, their one-dimensional composition profiles along the direction indicated in Fig. 5(a) inside the GB plane show synchronous fluctuations (Fig. 5(c)). In GB regions where Ni and Mn strongly co-segregate, the corresponding compositions of the other elements, Fe, Co and Cr fluctuate periodically in antiphase with Ni and Mn (Fig. 5(c)). The contour color profiles viewed from the GB normal further demonstrate the characteristic compositional modulation of Ni and Mn along the GB (Fig. 5(d and e)). The patterns and contour profiles all reveal a clear periodicity of the compositional fluctuations, resembling the confined spinodal fluctuations observed before in Fe-Mn alloys [27].

The periodic redistribution of the elements along the GB plane also occurs in samples aged for longer time. As an example, the corresponding results and the same type of periodic compositional fluctuations for a sample aged for 18 h are revealed using a set of iso-composition surfaces with threshold at 25.5 at. % Ni (Fig. 6(a)) and 19.5 at. % Mn (Fig. 6(b)), respectively, together with the one-dimensional composition profile (Fig. 6(c)) and two-dimensional contour map (Fig. 6(d and e)) along the GB. Although the GB segregations of Ni and Mn present a similar pattern in the samples aged for 6 and 18 h, their degrees of segregations are different. The degrees of segregation are higher and the sizes of some local

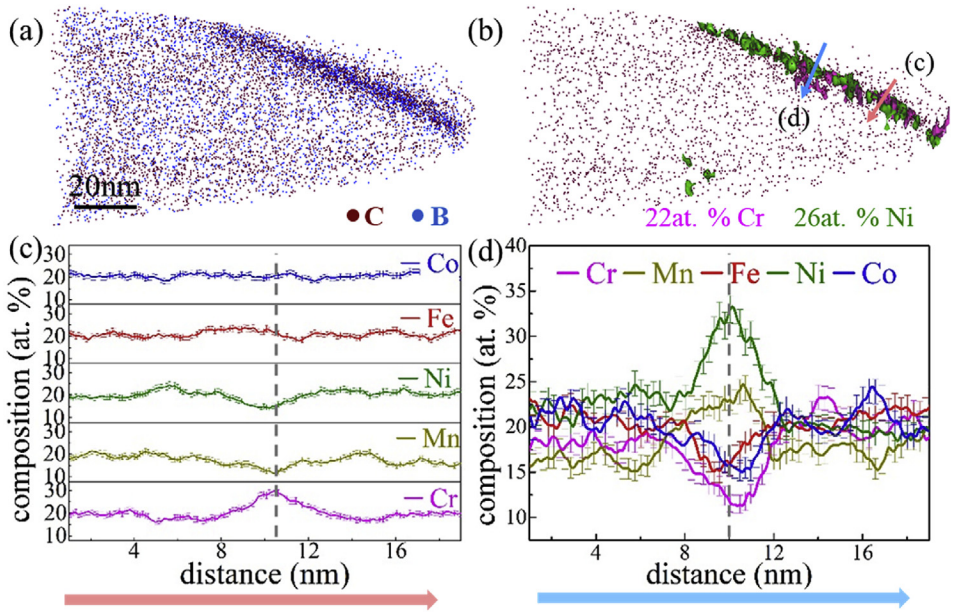


**Fig. 2.** Chemical composition of the FeMnNiCoCr grain boundary after aging treatment at 450 °C for 6 h. (a) C and B segregations at the GB, (b) 22 at. % Cr and 26 at. % Ni iso-composition surfaces with C atoms. (c) The one dimensional composition profiles taken along the direction indicated by the light-red arrow (across a highly Cr enriched GB region) shown in (b). (d) The one-dimensional composition profiles taken along the direction indicated by the light-blue arrow (across a highly Ni and Mn enriched GB region) shown in (b). The GB is viewed edge-on in (a,b) and the vertical dashed lines in (c,d) represent the approximate GB position. (For interpretation of the references to color in this figure legend, the reader is referred to the Web version of this article.)

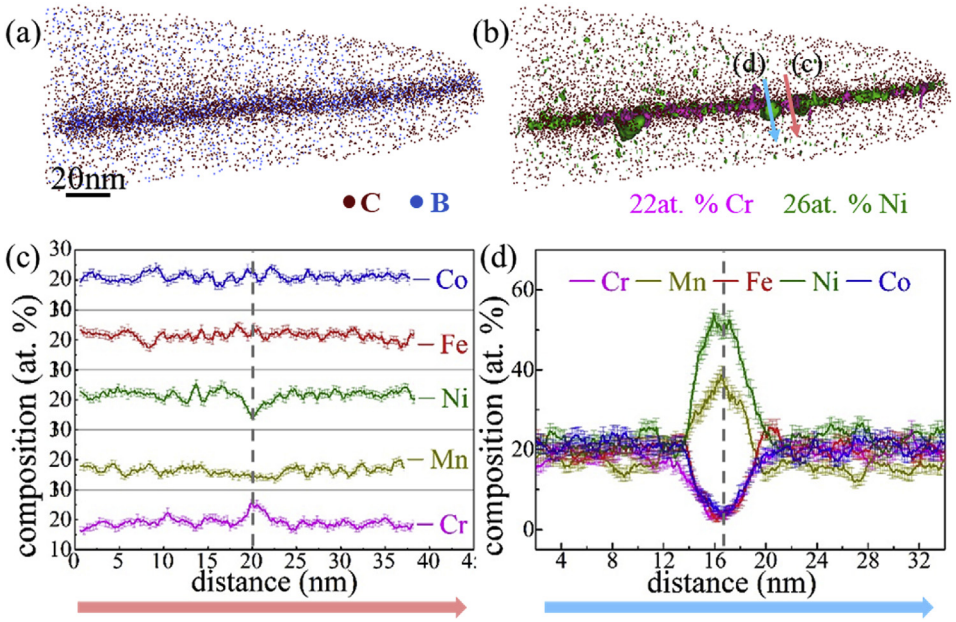


**Fig. 3.** Chemical composition of the FeMnNiCoCr grain boundary after aging at 450 °C for 18 h. (a) C and B segregations at the GB, (b) 22 at. %Cr and 26 at. %Ni iso-composition surfaces with C atoms. (c) The one dimensional composition profiles taken along the direction indicated by the light-red arrow (across a highly Cr enriched GB region) shown in (b). (d) The one-dimensional composition profiles taken along the direction indicated by the light-blue arrow (across a highly Ni and Mn enriched GB region) shown in (b). The GB is viewed edge-on in (a,b) and the vertical dashed lines in (c,d) represent the approximate GB position. (For interpretation of the references to color in this figure legend, the reader is referred to the Web version of this article.)

segregation regions are larger at the GBs when the sample is aged for longer time as analyzed in the following.

### 3.4. Temporal evolution of the elemental distribution within GBs

During aging for 6–48 h, the compositional modulations along the GBs gradually evolve (Fig. 7). Fig. 7(a) shows the 26 at. % Ni and 15 at. % Cr iso-composition surfaces at the GBs in the sample of as-received state. Fig. 7(b–d) shows 26 at. % Ni and 22 at. % Cr iso-composition surfaces at the GB in the samples aged for 6, 18 and 48 h, respectively. A higher threshold of the iso-composition surface is used for Cr in the aged states because Cr starts to segregate to the GBs only as aging proceeds. Based on the iso-composition surfaces of the as-received (Fig. 7(a)) and aged samples

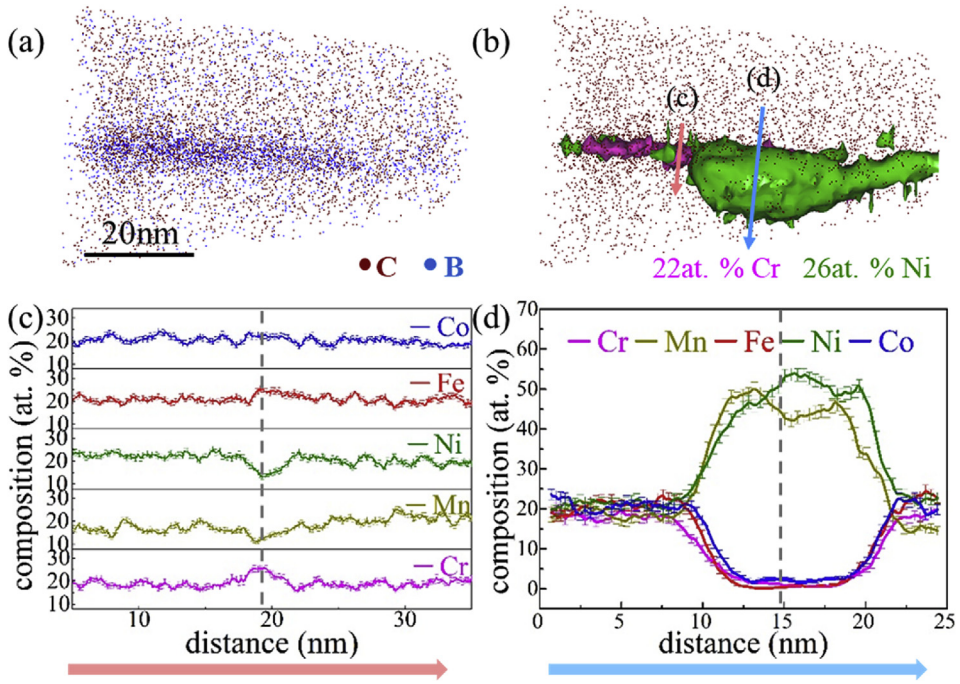


**Fig. 4.** Chemical composition of the FeMnNiCoCr grain boundary after aging treatment at 450 °C for 48 h. (a) C and B segregations at the GB, (b) 22 at. % Cr and 26 at. % Ni iso-composition surfaces with C atoms. (c) The one dimensional composition profiles taken along the direction indicated by the light-red arrow (across a highly Cr enriched GB region) shown in (b). (d) The one-dimensional composition profiles taken along the direction indicated by the light-blue arrow (across a highly Ni and Mn enriched GB region) shown in (b). The GB is viewed edge-on in (a,b) and the vertical dashed lines in (c,d) represent the approximate GB position. (For interpretation of the references to color in this figure legend, the reader is referred to the Web version of this article.)

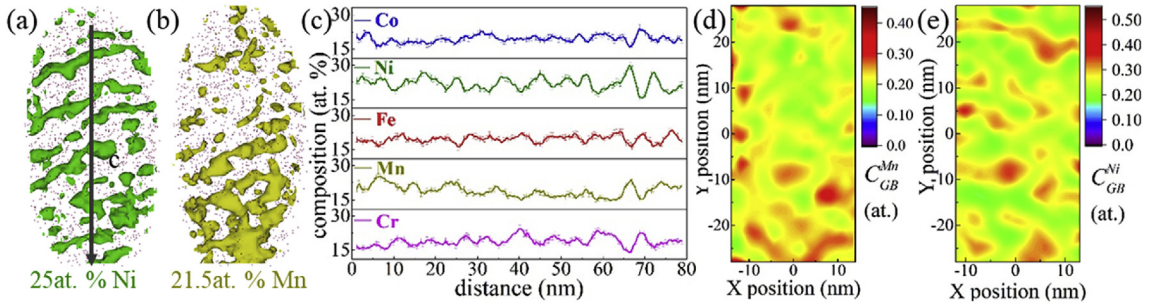


**Fig. 5.** Compositional modulation along the grain boundary in the FeMnNiCoCr alloy aged at 450 °C for 6 h. (a) 25 at. % Ni and (b) 21.5 at. % Mn iso-composition surfaces, (c) the one-dimensional composition profile along the direction indicated by the arow within the GB plane in (a). The two-dimensional contour color profiles of GB composition of (d) Mn and (e) Ni within the GB plane. (For interpretation of the references to color in this figure legend, the reader is referred to the Web version of this article.)

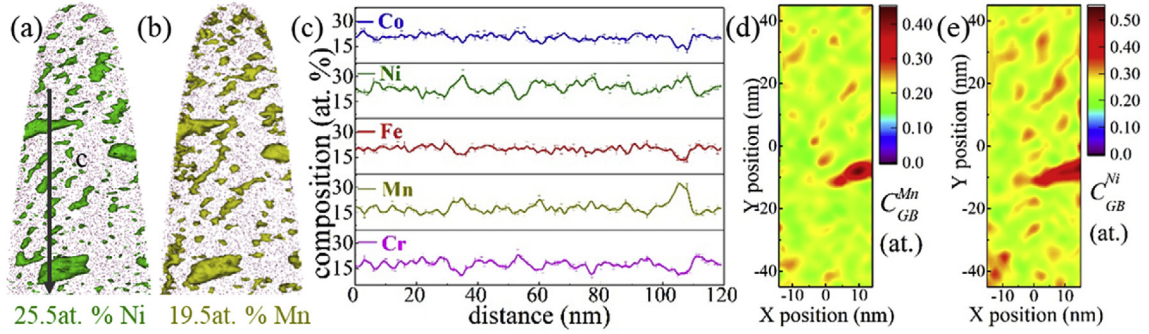


**Fig. 6.** Compositional modulation along the grain boundary in the FeMnNiCoCr alloy aged at 450 °C for 18 h. (a) 25.5 at. % Ni and (b) 19.5 at. % Mn iso-composition surfaces, (c) one-dimensional composition profile along the direction indicated by the arow within the GB plane in (a). The two-dimensional contour color profiles of GB composition of (d) Mn and (e) Ni within the GB plane. (For interpretation of the references to color in this figure legend, the reader is referred to the Web version of this article.)

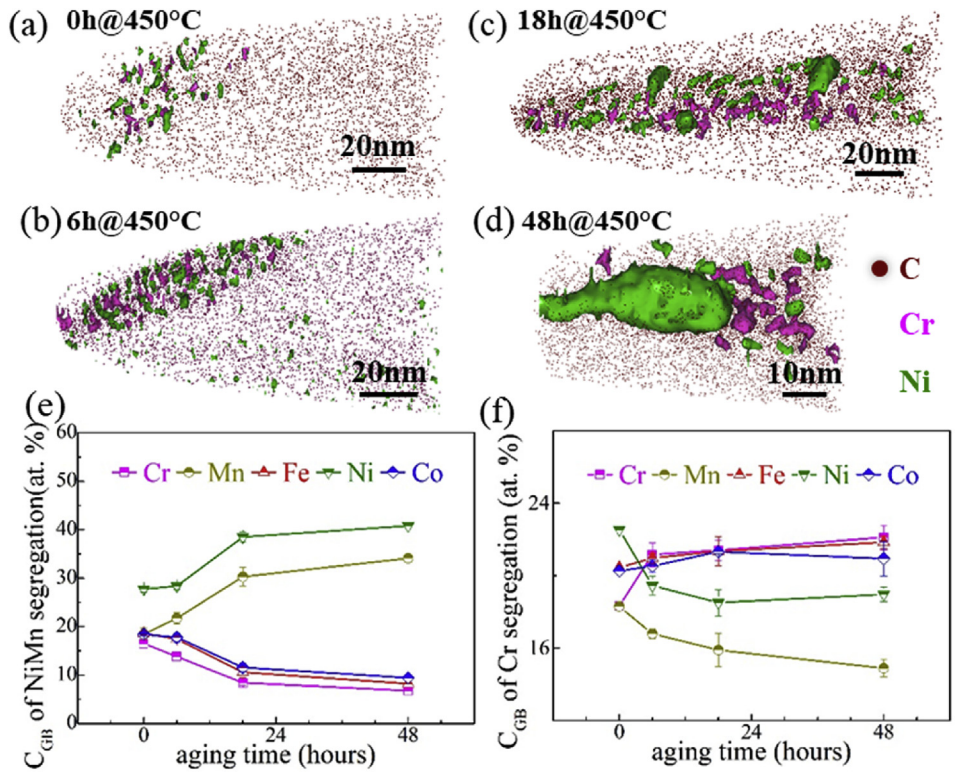


**Fig. 7.** Grain boundary compositions (CGB) in Ni + Mn rich regions and in Cr rich regions inside the interface and their variation with aging time. (a) 26 at. % Ni and 15 at. % Cr iso-composition surfaces at the GB (annealed state). (b) 26 at. % Ni and 22 at. % Cr iso-composition surfaces at the GB (450 °C for 6 h). (c) 26 at. % Ni and 22 at. % Cr iso-composition surfaces at a GB (450 °C for 18 h). (d) 26 at. % Ni and 22 at. % Cr iso-composition surfaces at a GB (450 °C for 48 h). (e) Influence of aging time on GB compositions in Ni + Mn rich GB regions. (f) Influence of aging time on GB compositions in Cr rich GB regions.

(Fig. 7(c–d)), we calculated the compositions of abundant segregation areas through analyzing composition profiles as a function of the distance to the iso-composition surface [41] in Fig. 7(e and f). The average instead of the maximum value of the composition profile was employed to measure the composition of the segregated elements.

Fig. 7(e) clearly shows that Ni starts to segregate at GBs in the as-received sample prior to aging (GB concentration is ~27.7 at. %), and, as aging proceeds at 450 °C, its GB composition steadily and monotonically increases over time (~28.4 at. % at 6 h, ~38.5 at. % at 18 h and 40.8 at. % at 48 h). Mn shows an increase while Fe, Co and Cr show a decrease in their GB concentrations over the course of aging. Such trend is consistent with the observations displayed in Figss. 2–4 that Ni and Mn undergo co-segregation in some regions of the GB that are depleted in Fe, Co and Cr. After aging for 48 h, the peak composition in the Ni and Mn rich regions reaches a value of $Ni_{50}Mn_{43.4}Cr_{2.1}Fe_{1.3}Co_{2.8}$ and retains constant for a certain distance (~dozens of nanometers), very close to that of the equilibrium NiMn phase reported earlier [7,8]. This present observation is thus interpreted as a 20 nm large nucleus of the NiMn equilibrium phase, which forms at the GBs in these co-segregation regions. With the spinodal precursors developing into new phases after long-time aging, the precursor GB compositional fluctuations gradually vanish as the elements partition into the new phases, leaving only a few small segregation areas behind as indicated in Fig. 7(d). At GB regions without segregation of Ni or Mn we find a slight Cr enrichment in the aged samples (Fig. 7(b–d)). As aging proceeds, the GB composition of Cr remains almost constant at a level far below that of the equilibrium Cr-rich phase [7,8] which means that this phase may need longer aging time to form at the GBs under the current imposed heat treatment condition.

## 4. Discussion

The uphill diffusion and the compositional modulations we observed for Ni and Mn in the GB plane of the FeMnNiCoCr HEA are similar to previous observations of spinodal decomposition phenomena along GBs in an Fe-Mn alloy [27] and in the bulk of Fe-Ni-Mn, Fe-Cr-Co and Fe-Cr alloys [42–45]. Also, phase separation phenomena through spinodal decomposition are very common in the bulk of HEAs [2,46–50]. For instance, by way of spinodal decomposition, Fe- and Cr-rich phases can form in an AlCoCrFeNi alloy [47], the ordered $L1_2$ phases form in the $Al_{0.5}Cr_{0.9}FeNi_{2.5}V_{0.2}$ alloy [48] and interconnected B2 and body-centered-cubic (bcc) microstructures form in $Fe_{30}Ni_{20}Mn_{25}Al_{25}$ [49] and $Al_{1.3}$CoCrCuFeNi [50]. Additionally, since miscibility gaps are common in the respective binary and ternary systems composed of the elements making up the present HEA [51–53], it is likely that a miscibility gap also exists in this quinary alloy.

To better understand the interfacial segregation, decomposition and phase nucleation processes, the segregation pattern of Ni and Mn has been analyzed in more detail (Fig. 8). The corresponding wavelengths and amplitudes of the periodic compositions (as indicated by the inset in Fig. 8(a)) were measured and analyzed statistically for all substitutional elements. We also quantified the compositional fluctuations in the grain interior for comparison and reference. The one-dimensional composition profiles are obtained from cylinders which lie in the GB plane and in the abutting grains. The compositional fluctuations in the grain interior are just statistical fluctuations and the segments in the grain interior of the above composition profiles (Figs. 1(d), 2(d), 3(d) and Fig. 4(d)) clearly show the random distributions of the component elements. The wavelengths (~2 nm) and amplitudes (~2 at. %) for all elements

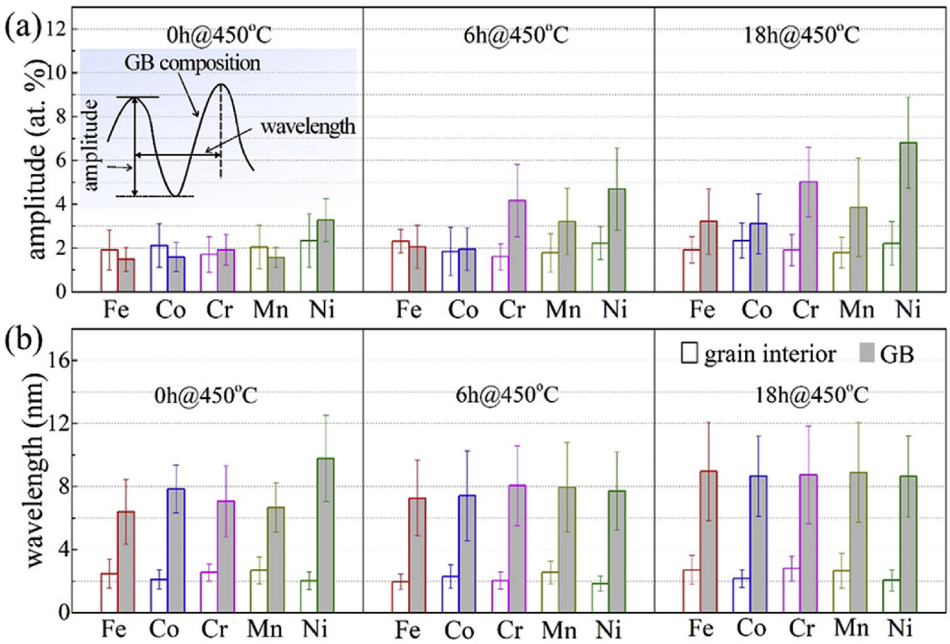


**Fig. 8.** Early evolution of random compositional fluctuation in the grain interior and the spinodal compositional modulation at the GBs as a function of aging time. (a) Amplitudes of the compositions in grain interior and at the GBs of the annealed sample, as well as the samples aged for 6 and 18 h. (b) Wavelengths of the compositions in grain interior and at the GBs of the as-received sample and the sample aged for 6 and 18 h. The amplitude shown here is the peak-to-peak amplitude.

remain stable during the annealing and aging treatments implying that no phase separation in the grain interior occurred. The higher wavelength (~6–10 nm) and the much higher amplitudes (~5–7 at. %) observed along the GBs are clearly different from those in the abutting grain interiors in both the absolute magnitudes and kinetics which increase as aging proceeds.

Here, with the observation of uphill diffusion and planar compositional modulations, we suggest that spinodal states occur on the decorated GBs with their locally enhanced Ni and Mn concentrations, but not in the grain interiors with their much smaller compositional fluctuations. The GB segregation and decomposition effects observed here are characterized by a gradual amplitude increase of the in-plane compositional fluctuations through uphill diffusion with an approximately steady wavelength (Fig. 8). This observation suggests that the GB phase separation in the current HEA is for ageing time between 0 and 18 h similar to the first stage of spinodal decomposition, characterized by a constant wavelength and increasing composition amplitudes [27,54,55].

Based on the Gibbs' adsorption isotherm, the linear and planar defects are thermodynamically susceptible to attract solutes to reduce the system's free energy [56]. The decrease in the Gibbs free energy of the GBs through segregation of Ni, Mn or Cr was observed before in experimental and theoretical studies of Fe-based alloys [57–60]. During the current aging process, Cr only shows segregations of low degrees to the GBs and it requires longer aging time to form a Cr-rich phase while Ni and Mn accumulating at the GBs gradually can induce the final phase nucleation with sufficient thermodynamic driving force. Also, in the present study, C and B segregate to the GBs, with the GB concentrations changing from 0.10 to 0.32 at. % for C and varying from 0.07 to 0.28 at. % for B. Their concentrations remain low, i.e. essentially at an impurity level, and they are always randomly distributed over all aging time. We found no connection between the random segregation behaviors of C and B with the spinodal segregation patterns of Ni and Mn at the GBs. This means that the minor C and B impurity content had no substantial influence on the segregation patterns and precursor states at the GBs.

Several authors such as Fowler, Guggenheim [61] and Guttmann [59] suggested adsorption models to account for preferential interactions between certain elements adsorbed to interfaces. These model variants allow for exploring effects such as elemental segregation, chemical decomposition and phase nucleation at GBs in multi-component systems [59–63]. Early studies also reveal that a free surface with high elemental enrichment can induce two-dimensional spinodal decomposition [64]. Further, due to the stress relaxation near surfaces, spinodal decomposition of surface modes can have faster kinetics than the corresponding bulk modes [65]. When considering such interactions in conjunction with reasonable approximations of the interaction energies, interfacial spinodal decomposition such as observed here can be understood in the context of classical alloy thermodynamics [30,61,66,67]. This indicates that the thermodynamic origins for the GB segregations are the same in conventional binary/ternary alloys as well as the current quinary alloy system. Yet, quantitative thermodynamic calculations of GB spinodal decompositions for the current multi-component system are challenging and the segregation proceeds via more complex diffusion, decomposition and partitioning pathways.

From these considerations and observations, we suggest a sequence for phase decomposition at the GBs in the current alloy: (i) Ni and Mn co-segregate to the GB. Cr, Fe and Co are depleted in the same regions but can enrich in other regions along the same GB. (ii) At other GB regions which are devoid of Ni and Mn segregations, Cr is the first of these elements that starts segregating to the GB. (iii) With further uphill diffusion inside the GB plane during aging, the Gibbsian enrichment in solutes, mainly Ni and Mn, shifts the local thermodynamic state of the GB into a spinodal regime of the (bulk) reference phase diagram. This effect leads to spinodal co-decomposition of Ni and Mn and the corresponding (anti-symmetric) co-depletion of Fe, Co and Cr at the GB. This means that the

two element groups Ni, Mn on the one hand and Cr, Fe, Co on the other hand form two opposite composition points of a spinodal decomposition in the 5-dimensional compositional phase space at 450 °C. (iv) These local spinodal enrichments forming on the GB plane act as compositional precursor states to the more stable equilibrium phases, one being the NiMn phase and the other one possibly being a Cr-rich phase.

GBs are usually regions of high disorder owing to their reduced atomic coordination and complex structure. When such segregation and depletion processes proceed, as in the current work, the compositional complexity at the GBs decreases. Ni tends to occupy sites neighboring to Mn instead of Fe, Co or Cr. Such preferential and accumulated bonding of Ni and Mn along the GBs generates a decrease in the configurational entropy and an increase in chemical order. The GBs thus reach a state of low entropy in contrast to the grain interiors with their stable and high compositional disorder in the current alloy of high entropy. The specific GB character may also play a role for GB segregation. For instance, regular segregation patterns may arise at coincidence site lattice (CSL) boundaries of high symmetry, such as at coherent twin boundaries [34] or faceted Σ9 tilt GBs [35]. Yet, for general high-angle GBs, which occupy a large fraction in metallic materials, segregation is less sensitive to the GB misorientations [68]. This means that for general high-angle GBs the trend for Gibbsian or respectively Fowler-Guggenheim GB decoration such as observed here is a first order effect while additional compositional modulations due to minor structural features of each interfaces are assumed to be second order effects.

## 5. Conclusions

In summary, we investigated compositional GB segregation and decomposition phenomena which play a fundamental role as precursor states for phase nucleation in the FeMnNiCoCr HEA. General high-angle GBs show strong Gibbsian co-segregation of Ni and Mn with corresponding co-depletion of Cr, Fe and Co. Cr shows slight enrichment in GB regions which are devoid of Ni or Mn segregation. The redistribution of these elements along the GB assumes the form of modulated compositional fluctuations. The segregation together with the associated compositional modulations constitute an increase in chemical order and thus entropy reduction in the GBs. While the grain interiors remain in a state of regular solid solution with high compositional disorder over all aging time, the Ni and Mn enrichments create spinodal precursor states for the subsequent phase nucleation at the GBs. These phenomena may lead to substantial changes in kinetics, energetics, GB properties and phase transformation in HEAs which altogether influence their macroscopic mechanical and functional behaviors. Thus, the current observations provide direct experimental evidences of regular segregation and compositional modulation phenomena on general high-angle GBs in multicomponent HEAs which can serve as spinodal precursor states for phase nucleation. These findings expand our knowledge on the local thermodynamics of lattice defects in complex solid solutions and help to provide implications for the design of advanced HEAs.

## Declarations of interest

None.

## Acknowledgement

This work has been financially supported by the Deutsche Forschungsgemeinschaft (SPP 2006). L.L is also supported by Alexander von Humboldt Stiftung and the China Scholarship Council.

## References

[1] B. Cantor, I.T.H. Chang, P. Knight, A.J.B. Vincent, Microstructural development in equiatomic multicomponent alloys, Mater. Sci. Eng. A 375–377 (2004) 213–218.
[2] J.W. Yeh, S.K. Chen, S.J. Lin, J.Y. Gan, T.S. Chin, T.T. Shun, C.H. Tsau, S.Y. Chang, Nanostructured high-entropy alloys with multiple principal elements: novel alloy design concepts and outcomes, Adv. Eng. Mater. 6 (2004) 299–303.
[3] B. Gludovatz, A. Hohenwarter, D. Catoor, E.H. Chang, E.P. George, R.O. Ritchie, A fracture-resistant high-entropy alloy for cryogenic applications, Science 345 (2014) 1153–1158.
[4] Z.M. Li, K.G. Pradeep, Y. Deng, D. Raabe, C.C. Tasan, Metastable high-entropy dual-phase alloys overcome the strength-ductility trade-off, Nature 534 (2016) 227–230.
[5] H. Luo, Z.M. Li, D. Raabe, Hydrogen enhances strength and ductility of an equiatomic high-entropy alloy, Sci. Rep. 7 (2017) 9892.
[6] O.N. Senkov, G.B. Wilks, J.N. Scott, D.B. Miracle, Mechanical properties of Nb25Mo25Ta25W25 and V20Nb20Mo20Ta20W20 refractory high entropy alloys, Intermetallics 19 (2011) 698–706.
[7] B. Schuh, F. Mendez-Martin, B. Völker, E.P. George, H. Clemens, R. Pippan, A. Hohenwarter, Mechanical properties, microstructure and thermal stability of a nanocrystalline CoCrFeMnNi high-entropy alloy after severe plastic deformation, Acta Mater. 96 (2015) 258–268.
[8] F. Otto, A. Dlouhý, K.G. Pradeep, M. Kuběnová, D. Raabe, G. Eggeler, E.P. George, Decomposition of the single-phase high-entropy alloy CrMnFeCoNi after prolonged anneals at intermediate temperatures, Acta Mater. 112 (2016) 40–52.
[9] E.J. Pickering, R. Muñoz-Moreno, H.J. Stone, N.G. Jones, Precipitation in the equiatomic high-entropy alloy CrMnFeCoNi, Scr. Mater. 113 (2016) 106–109.
[10] A.P. Sutton, R.W. Balluffi, Interfaces in Crystalline Materials, Clarendon Press, 1995.
[11] E.O. Hall, The deformation and ageing of mild steel: III discussion of results, Proc. R. Soc. Ser. B 64 (1951) 747–753.
[12] N.J. Petch, The cleavage strength of polycrystals, J. Iron Steel I 174 (1953) 25–28.
[13] A. Khalajhedayati, Z. Pan, T.J. Rupert, Manipulating the interfacial structure of nanomaterials to achieve a unique combination of strength and ductility, Nat. Commun. 7 (2016) 10802.
[14] L. Lu, Y. Shen, X. Chen, L. Qian, K. Lu, Ultrahigh strength and high electrical conductivity in copper, Science 304 (2004) 422–426.
[15] A. King, G. Johnson, D. Engelberg, W. Ludwig, J. Marrow, observations of intergranular stress corrosion cracking in a grain-mapped polycrystal, Science 321 (2008) 382–385.
[16] E. Bonetti, L. Del Bianco, D. Fiorani, D. Rinaldi, R. Caciuffo, A. Hernando, Disordered magnetism at the grain boundary of pure nanocrystalline iron, Phys. Rev. Lett. 83 (1999) 2829–2832.
[17] T. Watanabe, An approach to grain boundary design for strong and ductile polycrystals, Res. Mech. 11 (1984) 47–84.
[18] D. Raabe, S. Sandlöbes, J. Millán, D. Ponge, H. Assadi, M. Herbig, P.P. Choi, Segregation engineering enables nanoscale martensite to austenite phase transformation at grain boundaries: a pathway to ductile martensite, Acta Mater. 61 (2013) 6132–6152.
[19] C.T. Liu, C.L. White, J.A. Horton, Effect of boron on grain-boundaries in Ni3Al, Acta Metall. 33 (1985) 213–229.
[20] T. Chookajorn, H.A. Murdoch, C.A. Schuh, Design of stable nanocrystalline alloys, Science 337 (2012) 951–954.
[21] J. Luo, H. Cheng, K.M. Asl, C.J. Kiely, M.P. Harmer, The role of a bilayer interfacial phase on liquid metal embrittlement, Science 333 (2011) 1730–1733.
[22] M.P. Seah, E.D. Hondros, Grain boundary segregation, Proc. R. Soc. A 335 (1973) 191–212.
[23] P. Lejcek, M. Sob, V. Paidar, Interfacial segregation and grain boundary embrittlement: an overview and critical assessment of experimental data and calculated results, Prog. Mater. Sci. 87 (2017) 83–139.
[24] A.R. Kalidindi, C.A. Schuh, Stability criteria for nanocrystalline alloys, Acta Mater. 132 (2017) 128–137.
[25] S.L. Ma, K.M. Asl, C. Tansarawiput, P.R. Cantwell, M.H. Qi, M.P. Harmer, J. Luo, A grain boundary phase transition in Si–Au, Scr. Mater. 66 (2012) 203–206.
[26] S.F. Yang, N.X. Zhou, H. Zheng, S.P. Ong, J. Luo, First-order interfacial transformations with a critical point: breaking the symmetry at a symmetric tilt grain boundary, Phys. Rev. Lett. 120 (2018) 085702.
[27] A. Kwiatkowski da Silva, D. Ponge, Z. Peng, G. Inden, Y. Lu, A. Breen, B. Gault, D. Raabe, Phase nucleation through confined spinodal fluctuations at crystal defects evidenced in Fe-Mn alloys, Nat. Commun. 9 (2018) 1137.
[28] M. Kuzmina, M. Herbig, D. Ponge, S. Sandlobes, D. Raabe, D., Linear complexions: confined chemical and structural states at dislocations, Science 349 (2015) 1080–1083.
[29] A. Kwiatkowski da Silva, G. Leyson, M. Kuzmina, D. Ponge, M. Herbig, S. Sandlöbes, B. Gault, J. Neugebauer, D. Raabe, Confined chemical and structural states at dislocations in Fe-9 wt. % Mn steels: a correlative TEM-atom probe study combined with multiscale modelling, Acta Mater. 124 (2017) 305–315.
[30] A. Kwiatkowski da Silva, R.D. Kamachali, D. Ponge, B. Gault, J. Neugebauer, D. Raabe, Thermodynamics of grain boundary segregation, interfacial spinodal and their relevance for nucleation during solid-solid phase transitions, Acta

Mater. 168 (2019) 109–120.
[31] G.D. Preston, Age-hardening of copper-aluminium alloys, Proc. Phys. Soc. 52 (1940) 77–79.
[32] A. Guinier, Structure of age-hardened aluminium-copper alloys, Nature 142 (1938) 569.
[33] H. Zhao, F. De Geuser, A. Kwiatkowski da Silva, A. Szczepaniak, B. Gault, D. Ponge, D. Raabe, Segregation assisted grain boundary precipitation in a model Al-Zn-Mg-Cu alloy, Acta Mater. 156 (2018) 318–329.
[34] J.F. Nie, Y.M. Zhu, J.Z. Liu, X.Y. Fang, Periodic segregation of solute atoms in fully coherent twin boundaries, Science 340 (2013) 957–960.
[35] C.H. Liebscher, A. Stoffers, M. Alam, L. Lymperakis, O. Cojocaru-Mirédin, B. Gault, J. Neugebauer, G. Dehm, C. Scheu, D. Raabe, Strain-Induced asymmetric line segregation at faceted Si grain boundaries, Phys. Rev. Lett. 121 (2018) 015702.
[36] N.X. Zhou, J. Luo, Grain boundary complexions in multicomponent alloys: challenges and opportunities, Curr. Opin. Solid State Mater. Sci. 20 (2016) 268–277.
[37] Z.R. Peng, Y.F. Lu, C. Hatzoglou, A. Kwiatkowski da Silva, F. Vurpillot, D. Ponge, D. Raabe, B. Gault, An automated computational approach for complete in-plane compositional interface analysis by atom probe tomography, Microsc. Microanal. (2019) 1–12.
[38] Z.W. Wang, I. Baker, W. Guo, J.D. Poplawsky, The effect of carbon on the microstructures, mechanical properties, and deformation mechanisms of thermo-mechanically treated Fe40.4Ni11.3Mn34.8Al7.5Cr6 high entropy alloys, Acta Mater. 126 (2017) 346–360.
[39] M. Herbig, D. Raabe, Y.J. Li, P. Choi, S. Zaefferer, S. Goto, Grain boundary segregation in Fe–Mn–C twinning-induced plasticity steels studied by correlative electron backscatter diffraction and atom probe tomography, Acta Mater. 83 (2015) 37–47.
[40] J.B. Seol, J.W. Bae, Z. Li, J.C. Han, J.G. Kim, D. Raabe, H.S. Kim, Boron doped ultrastrong and ductile high-entropy alloys, Acta Mater. 151 (2018) 366–376.
[41] O.C. Hellman, J.A. Vandenbroucke, J. Rusing, D. Isheim, D.N. Seidman, Microsc. Microanal. 6 (2000) 437–444.
[42] W.K. Choo, J.H. Kim, J.C. Yoon, Microstructural change in austenitic Fe-30.0wt%Mn-7.8wt%Al-1.3wt%C initiated by spinodal decomposition and its influence on mechanical properties, Acta Mater. 45 (1997) 4877–4885.
[43] M.K. Miller, J.M. Hyde, M.G. Hetherington, A. Cerezo, G.D.W. Smith, C.M. Elliott, Spinodal decomposition in Fe-Cr alloys: experimental study at the atomic level and comparison with computer models—I. Introduction and methodology, Acta Metall. Mater. 43 (1995) 3385–3401.
[44] J. Singh, C.M. Wayman, Age-hardening characteristics of a martensitic Fe-Ni-Mn alloy, Mater. Sci. Eng. 94 (1987) 233–242.
[45] F. Zhu, P. Haasen, R. Wagner, An atom probe study of the decomposition of Fe-Cr-Co permanent magnet alloys, Acta Metall. 34 (1986) 457–463.
[46] C.J. Tong, Y.L. Chen, S.K. Chen, J.W. Yeh, T.T. Shun, C.H. Tsau, S.J. Lin, S.Y. Chang, Microstructure characterization of AlxCoCrCuFeNi high-entropy alloy system with multiprincipal elements, Metall. Mater. Trans. A 36A (2005) 881–893.
[47] A. Manzoni, H. Daoud, R. Völkl, U. Glatzel, N. Wanderka, Phase separation in equiatomic AlCoCrFeNi high-entropy alloy, Ultramicroscopy 132 (2013) 212–215.
[48] Y.J. Liang, L.J. Wang, Y.R. Wen, B.Y. Cheng, Q.L. Wu, T.Q. Cao, Q. Xiao, Y.F. Xue, G. Sha, Y.D. Wang, Y. Ren, X.Y. Li, L. Wang, F.C. Wang, H.N. Cai, High-content ductile coherent nanoprecipitates achieve ultrastrong high-entropy alloys, Nat. Commun. 9 (2018) 4063.
[49] J.A. Hanna, I. Baker, M.W. Wittmann, A new high-strength spinodal alloy, J. Mater. Res. 20 (2005) 791–795.
[50] L.J. Santodonato, Y. Zhang, M. Feygenson, C.M. Parish, M.C. Gao, R.J.K. Weber, J.C. Neuefeind, Z. Tang, P.K. Liaw, Deviation from high-entropy configurations in the atomic distributions of a multi-principal-element alloy, Nat. Commun. 6 (2015) 5964.
[51] T. Suzuki, Metastable miscibility gap island in Fe-Ni-Mn ternary martensitic alloys, Trans. Jpn. Inst. Met. 11 (1970) 257–263.
[52] H. Kaneko, M. Homma, K. Nakamura, M. Okada, G. Thomas, Phase diagram of Fe-Cr-Co permanent magnet system, IEEE Trans. Magn. 13 (1977) 1325–1327.
[53] J.O. Andersson, B. Sundman, Thermodynamic properties of the Cr-Fe system, Calphad 11 (1987) 83–92.
[54] J.W. Cahn, On spinodal decomposition, Acta Metall. 9 (1961) 795–801.
[55] J.W. Cahn, Spinodal decomposition, Trans. Metall. Soc. AIME 242 (1968) 166–180.
[56] R. Kirchheim, Acta Mater. 55 (2007) 5129–5138.
[57] P. Lejček, Grain Boundary Segregation in Metals, Springer, 2010.
[58] E.D. Hondros, M.P. Seah, The theory of grain boundary segregation in terms of surface adsorption analogues, Metall. Trans. A 8 (1977) 1363–1371.
[59] M. Guttmann, Equilibrium segregation in a ternary solution: a model for temper embrittlement, Surf. Sci. 53 (1975) 213–227.
[60] P. Gas, M. Guttmann, J. Bernardini, The interactive co-segregation of Sb and Ni at the grain boundaries of ultra-high purity Fe-base alloys, Acta Metall. 30 (1982) 1309–1316.
[61] R.H. Fowler, E.A. Guggenheim, Statistical Thermodynamics, Cambridge University Press, New York, 1939.
[62] M. Guttmann, P. Dumoulin, M. Wayman, The thermodynamics of interactive co-segregation of phosphorus and alloying elements in iron and temper-brittle steels, Metall. Trans. A 13 (1982) 1693–1711.
[63] P. Wynblatt, D. Chatain, Modeling grain boundary and surface segregation in multicomponent high-entropy alloys, Phys. Rev. Mater. 3 (2019) 054004.
[64] C. Geng, L.Q. Chen, Spinodal decomposition and pattern formation near a crystalline surface, Surf. Sci. 355 (1996) 229–240.
[65] M. Tang, A. Karma, Surface modes of coherent spinodal decomposition, Phys. Rev. Lett. 108 (2012) 265701.
[66] J.W. Cahn, Transitions and phase equilibria among grain boundary structures, J. Phys. Colloq. 43 (1982) 199–213.
[67] E.W. Hart, Two-dimensional phase transformation in grain boundaries, Scr. Metall. 2 (1968) 179–182.
[68] M. Herbig, D. Raabe, Y.J. Li, P. Choi, S. Zaefferer, S. Goto, Atomic-scale quantification of grain boundary segregation in nanocrystalline material, Phys. Rev. Lett. 112 (2014) 126103.